2012

Spring-Block Models of Earthquake Dynamics

Ashley E. McCall
Minnesota State University - Mankato

Spring-Block Models of Earthquake Dynamics

by

Ashley McCall

A Thesis Submitted in Partial Fulfillment of the Requirements for the Degree of

Master of Arts

In

Mathematics

Minnesota State University, Mankato

Mankato, Minnesota

May 2012

May, 2012

This Thesis has been examined and approved.

Examining Committee:

Dr. Brian Martensen, Chairperson

Dr. Ruijun Zhao

Dr. Bryce Hoppie

Abstract

In this paper, the dynamics of spring-block models are studied. A brief overview of the history of spring-block models relating to earthquakes is presented, along with the development of friction laws. Several mathematical topics relating to dynamical systems are also discussed. We consider two spring-block models; one with Dieterich-Ruina rate and state dependent friction and another with a modified Dieterich-Ruina style friction. For each system, the qualitative behavior and numerical solutions are presented. In the first case, we find that the system undergoes a Hopf bifurcation from a stationary solution to a periodic orbit, and eventually transitions to chaos. In the latter case, we find that a stationary solution exists along with the conditions for a Hopf bifurcation to occur. We develop the mathematical framework to compute periodic and chaotic behavior for the system. Future work will be to develop more efficient algorithms to perform the actual computations.

Table of Contents

Table of Figures

Nomenclature

θ	State Variable
u	Slip
v	Velocity
v_0	Reference Velocity
D_c	Critical Sliding Distance
k	Spring Constant
M	Mass Block
A	Empirical Constant
B	Empirical Constant
c	Viscous Damping Constant
η	Nondimensional Viscous Damping Constant
ϵ	Sensitivity to velocity relaxation $\left(= \frac{B-A}{A}\right)$
ξ	Nondimensional Spring Constant $\left(= \frac{kD_c}{A}\right)$
γ	Nondimensional Frequency $\left(= \sqrt{\frac{k}{M}}\left(\frac{D_c}{v_0}\right)\right)$

Chapter 1

Introduction

For many years earthquakes were understood soley through laboratory models and theory. Seismology lacked a mathematical foundation upon which computations could be made. As a result, there was no comparison for the quantitative features of theory and the observations in nature. Burridge and Knopoff sought to construct a mathematical description of earthquake mechanism and the correlation between sequential earthquakes in time and space. In particular, they were interested in the role that friction played in regard to earthquake mechanism [BK67].

Earthquakes occur on pre-existing faults. Burridge and Knopoff demonstrated that a slider-block pulled by a spring can be used to model the behavior of an earthquake fault. The slider block is coupled by a spring to a velocity driver, as depicted in Figure 1.1. The block interacts with the rough surface through friction. The frictional force holds the block in place until it is overcome by the force of the spring. Once the frictional resistance is surpassed by the spring, slip occurs. The slip represents an earthquake on a fault. The extension of the spring represents the elastic strain in the rock adjacent to the fault. This behavior is classified as stick-slip behavior [Tur97].

Burridge and Knopoff's model analyzed the equations of motion, taking into account the frictional interaction of the block and the surface upon which the block

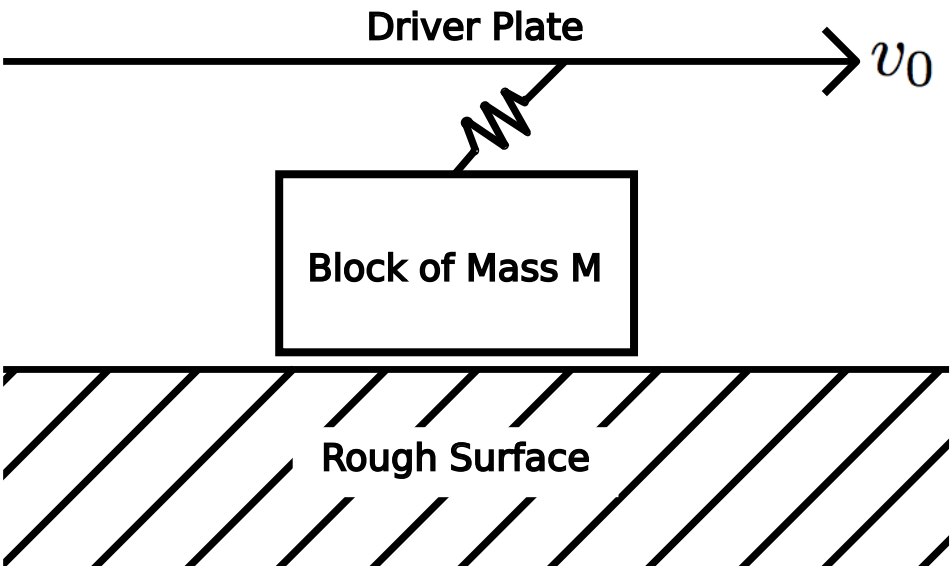

Figure 1.1: Spring-Block Model

slips. Their friction term was a linear function of velocity which included the effects of instability, seismic radiation, and viscosity [BK67]. Many studies have been done on these spring-block models. There have been numerous attempts at improving the models in order to produce more realistic fault behavior. It has been shown that one of the most important factors in laboratory model improvement is the friction constitutive laws [EL08]. The introduction of slip rate and state variable constitutive laws for rock friction by Dieterich, Ruina, and Rice in the 1980s form a basis for the friction laws commonly used today. By studying constitutive friction laws, it was determined that a simple velocity-dependent friction law was not adequate in replicating the behavior of a fault [Mar98]. Thus, the friction law used by Burridge and Knopoff needed modification. Using the laboratory-derived friction laws, Dieterich, Ruina, Rice, and others made improvements to the friction laws used by Burridge and Knopoff [EL08]. While earlier friction laws limited

modeling laboratory data and seismic behaviors, such as repeated stick-slip failure and the seismic cycle, the incorporation of the rate and state friction laws resolved these problems [Mar98]. By incorporating the state variable, traits characteristic of faulting, such as stick-slip phenomena, fault healing, and memory effects were exhibited by models. The state variable is often interpreted as the amount of asperity contact between the model block and the surface upon which it slides. Fault healing refers to the process by which a fault recovers its strength due to the increase of static friction, whereas memory effects refers to the idea that the recurrence time of previous of earthquakes plays an important role in fault rupture [EL08], [Sch02]. For more details on model improvement and friction laws see Marone [Mar98].

In Chapter 2 we begin with an overview of the mathematics involved in this paper. Chapter 3 will examine the model from Erickson's paper, a model which was originally proposed by Raúl Madariaga [EL08]. This spring block model uses Dieterich-Ruina style friction, which takes into account the previously mentioned slip rate and state variable. In addition, Dieterich-Ruina style friction incorporates a logarithmic term. As we will see, this nonlinear term poses added difficulty in solving the problem [EL08]. Then, in Chapter 4, we will propose a modified version of the model introduced in Chapter 3. For the modified model, we will examine the dynamics and compare them with the dynamics of the model in Chapter 3. We will conclude the paper by discussing future work.

Chapter 2

Preliminaries

The motion of the spring-block can be modeled by a system of ordinary nonlinear differential equations. In order to analyze the dynamics of this system, we first must be familiar with the mathematics involved. Commonly, systems of ordinary differential equations (ODEs) are difficult, if not impossible, to solve analytically. Due to this characteristic, we often analyze the problem in terms of qualitative features. To perform a qualitative analysis of the system, we must be familiar with certain concepts, such as nondimensionalization, fixed points and their stability, bifurcation theory, Poincaré maps, chaos, and Lyanpunov exponents. Chapter 2 will begin with an overview of these concepts. Since the system we are working with cannot be solved analytically, we will also need to discuss numerical methods and how they apply to the problem. Lastly, when the modified system is introduced, we will find a need to approximate a discontinuous function. We will introduce a mollifier, which allows us to provide a smooth approximation for our discontinuous function.

2.1 Nondimensionalization

A useful technique in analyzing a first-order system is to express the system of equations in dimensionless form. By creating a dimensionless system, we are able to define small as being much less than 1. In addition, nondimensionalizing the system reduces the number of parameters [Str94]. To put a system into nondimensional form, we must nondimensionalize each equation. The two-step procedure outlined by Lin and Segel [LS74] can be generalized to a system of equations. First, we make a list of all the parameters and variables in the system, making note of their dimensions. Next, we examine each variable. For each variable, we must form a combination of parameters with the same dimension as the variable. Typically, there is more than one way to form this combination of parameters. For example, let x be a variable and let p be a combination of parameters with the same dimension as x. Introduce the nondimensional variable, $\hat{x}$, and set $\hat{x} = x/p$. Equivalently, we could write $x = p\hat{x}$. We must nondimensionalize time in the same way, whether our differential equation is autonomous or non-autonomous. Once we have defined our dimensionless variables, it is a matter of substitution into the system of equations. This substitution requires the chain rule [LS74]. To express the derivatives with respect to the new time, we must implement the chain rule. For instance,

$$\dot{x} = \frac{dx}{dt} = \frac{dx}{d\hat{t}}\frac{d\hat{t}}{dt} \tag{2.1}$$

where $\hat{t}$ is the dimensionless time [Str94]. We do this for each equation and substitute the new dimensionless variables and parameters as appropriate. Once the

substitutions are complete, it is common to carry out further calculations and form new dimensionless parameters [LS74]. New dimensionless parameters are formed by grouping the original parameters [Str94]. These new dimensionless parameters are often referred to as dimensionless groups. A properly nondimensionalized problem will yield only dimensionless groups [LS74]. In this paper, we will take our system of nonlinear ODEs and work through the steps to nondimensionalize it. Using this dimensionless system, we will then be able to examine several qualitative features of the system, such as equilibria and their stabilities, as well as bifurcations.

2.2 Fixed Points and Stability

For a given system of equations of the form

$$\begin{aligned} \dot{x_1} &= f_1(x_1, x_2, ..., x_n) \\ \dot{x_2} &= f_2(x_1, x_2, ..., x_n) \\ &\vdots \\ \dot{x_n} &= f_n(x_1, x_2, ..., x_n) \end{aligned} \tag{2.2}$$

where each f_i is a given function, we can perform qualitative analyses. The system can be written more compactly as

$$\dot{\mathbf{x}} = \mathbf{f}(\mathbf{x}) \tag{2.3}$$

where $\mathbf{x} = (x_1, x_2, ..., x_n)$ and $\mathbf{f}(\mathbf{x}) = (f_1(\mathbf{x}), f_2(\mathbf{x}), ..., f_n(\mathbf{x}))$. Fixed points, $\mathbf{x}^*$, of the system satisfy $\mathbf{f}(\mathbf{x}^*) = \mathbf{0}$. Fixed points represent steady states or equilibria of the system. Another prominent feature of the system is closed orbits, which represent

periodic solutions. In other words, closed orbits occur when $\mathbf{x}(t+T) = \mathbf{x}(t)$ for all t, for some $T > 0$. Due to this property, closed orbits are often referred to as periodic orbits. The stability or instability of these fixed points and periodic orbits are of interest in analyzing the dynamics of a system. To obtain information about stabilities, we look to linearizing the system. By linearizing the system, we are able to use the Jacobian in our computations. Computing the eigenvalues of the Jacobian matrix at each fixed point will determine the stability of each fixed point. The Jacobian, J, is a matrix of first partial derivatives of each f_i:

$$J(\mathbf{x}) = \begin{pmatrix} \frac{\partial f_1}{\partial x_1} & \frac{\partial f_1}{\partial x_2} & \cdots & \frac{\partial f_1}{\partial x_n} \\ \frac{\partial f_2}{\partial x_1} & \frac{\partial f_2}{\partial x_2} & \cdots & \frac{\partial f_2}{\partial x_n} \\ \vdots & \vdots & \ddots & \vdots \\ \frac{\partial f_n}{\partial x_1} & \frac{\partial f_n}{\partial x_2} & \cdots & \frac{\partial f_n}{\partial x_n} \end{pmatrix} \tag{2.4}$$

Let A denote the Jacobian evaluated at a fixed point. The eigenvalues of A will determine the stability of a fixed point. The eigenvalues of A can be found by solving the characteristic equation $det(A - \lambda I) = 0$ for λ, where λ is an eigenvalue of A and I is the identity matrix. If all of the eigenvalues of A have a positive real part, then the fixed point can be classified as a source, or a repeller. When all of the eigenvalues of A have a negative real part, the fixed point is a sink, or an attractor. If some of the eigenvalues of A have a positive real part, while the rest have a negative real part, we classify the fixed point as a saddle. Sinks are stable, whereas sources and saddles are unstable [Str94], [Wig03]. There are also marginal cases to consider, and these occur when at least one eigenvalue has a real part equal to zero. In some of these marginal cases we may encounter centers, meaning the fixed

point is surrounded by closed orbits. However, in marginal cases the linearization may incorrectly predict the local behavior of the system. Eigenvalues with a zero real part often coincide with a change of stability in the system [Str94].

2.3 Bifurcations

It is possible for fixed points and periodic orbits of a system to be created, destroyed, or to even change stability. Bifurcations represent qualitative changes in the dynamics of a system. As some control parameter is varied, bifurcations show the transitions or instabilities of a system. Bifurcations can also describe how oscillations can be turned on or off [Str94]. In this paper, we will be interested in a particular type of bifurcation known as a Hopf bifurcation. A Hopf bifurcation occurs when a periodic orbit surrounding a fixed point emerges from the fixed point [Str94]. Figure 2.1 shows a Hopf bifurcation in a plane. From left to right, the first image shows a stable fixed point, x^*. In the middle image, the fixed point loses its stability and a stable periodic orbit begins to grow from the fixed point. The final image displays the attracting periodic orbit that bifurcated from the now unstable fixed point.

We are interested in the case where the matrix A from Section 2.2 has a pair of purely imaginary eigenvalues with the remaining eigenvalues having nonzero real parts. Hence, if we have a system with a pair of complex eigenvalues and all other eigenvalues with a nonzero real part, there is a chance the system may undergo a Hopf bifurcation [Str94], [Wig03]. When a pair of complex conjugate eigenvalues cross the imaginary axis, the fixed point will bifurcate into a periodic orbit, thus

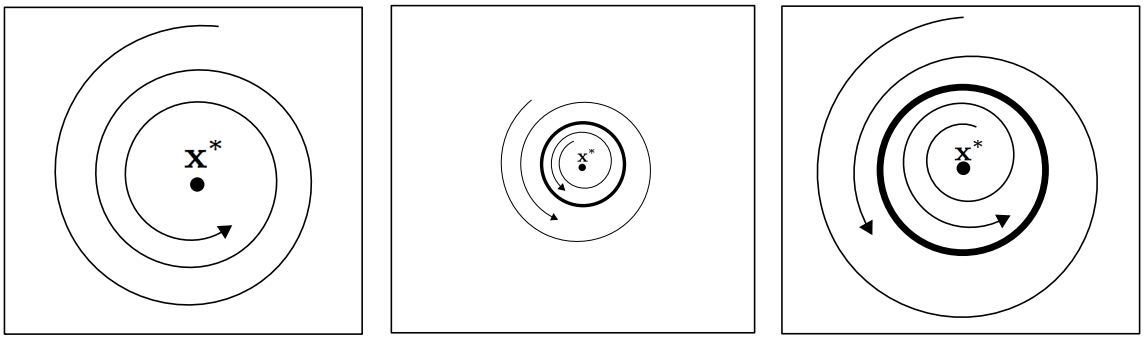

Figure 2.1: Hopf Bifurcation

changing the dynamics of the system [EL08], [Str94], [Wig03].

In this paper, we will see that each system undergoes a Hopf bifurcation, meaning for certain parameter values the spring-block model has a stable fixed point. As the parameters are varied, this fixed point loses its stability and a stable periodic orbit grows from the fixed point. The Hopf bifurcation will be evident in our numerical simulations. A period doubling bifurcation also occurs [EL08], meaning that a period n orbit loses its stability and from it, a period $2n$ orbit is produced. The periodic orbit that forms as the result of a Hopf bifurcation will be a period one orbit. We will witness the period one orbit bifurcating into a period 2 orbit, a period 2 orbit bifurcating into a period 4 orbit, and so on [EL08]. However, the period doubling bifurcations are not as obvious in our numerical simulations. We will rely on Poincaré maps to determine the period of an orbit.

2.4 Poincaré Maps

Using a Poincaré map, a continuous time system may be viewed as a discrete time system. Poincaré maps are advantageous in several ways when it comes to

studying ordinary differential equations. Not only do Poincaré maps reduce the dimension of the problem, but they also offer insight to the global dynamics of the system. These maps will be particularly useful in that they allow us to deduce the stability properties of periodic orbits [Wig03]. Recall the n-dimensional system (2.3). Consider a periodic solution in the n-dimensional phase space. Let S be an $(n-1)$-dimensional local cross section of a periodic solution which is transverse to the flow [GH90], [Str94]. In other words, the flow runs through S, and not parallel to S. We are interested in the points at which the flow trajectory intersects S. The Poincaré map, P, is a mapping from S to itself, defined by $\mathbf{x}_{k+1} = P(\mathbf{x}_k)$, where $\mathbf{x}_k \in S$ is the *kth* intersection, as is shown in Figure 2.2. A fixed point of P corresponds to a period one orbit in the phase space. Period two orbits will produce two points in P, and in general, a period p orbit will appear as p points in the Poincaré map. Randomly distributed points will represent chaotic orbits. Typically, fixed points of (2.3) will not appear on P [EL08], [Str94]. While Poincaré maps are useful, it is difficult or often impossible, to find a formula for P [Str94]. Thus, we rely on numerical methods to produce a Poincaré map.

2.5 Chaos

Although there is currently no universally accepted definition for chaos, there is a general consensus on the three elements used in the following definition: "Chaos is aperiodic long-term behavior in a deterministic system that exhibits sensitive dependence on initial conditions" [Str94]. "Aperiodic long-term behavior" implies that the system has trajectories which do not settle down to fixed points or periodic

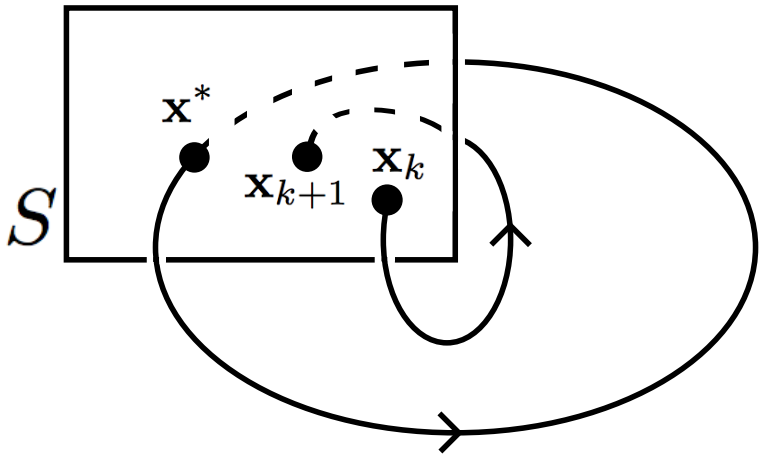

Figure 2.2: Poincaré Map

orbits. In other words, there are no attracting fixed points or periodic orbits in the system. A "deterministic" system is one in which there are no random or noisy inputs or parameters. This implies that the irregular behavior of the system is due to its nonlinearity. "Sensitive dependence on initial conditions" means that two trajectories that start close together may rapidly diverge from each other, making it difficult to predict the long term behavior of a system. An attractor is an invariant set in which all neighboring trajectories converge. Sinks and stable period orbits are examples of attractors. There is another kind of attractor, known as a strange attractor, or chaotic attractor. A strange attractor exhibits sensitive dependence on initial conditions. In a strange attractor, solutions oscillate in an irregular fashion, never exhibiting periodic behavior or settling down to fixed points, but always remaining in a bounded region of the phase space [Str94]. As mentioned previously, we will encounter sinks and stable periodic orbits for certain parameter values. In addition we will encounter a strange attractor [EL08]. To verify that this attractor is strange, we must determine if it exhibits sensitive dependence on initial

conditions. One method for determining if a system exhibits sensitive dependence on initial conditions is by computing the Lyapunov exponents of the system.

2.6 Lyapunov Exponents

Computing the Lyapunov exponents of a system will indicate whether or not the system is chaotic. Lyapunov exponents represent the rate at which neighboring trajectories separate. An n-dimensional system can have up to n distinct Lyapunov exponents [Str94]. For a given point on an attractor, $\mathbf{x}(t)$, at time t, consider a nearby point, $\mathbf{x}(t) + \delta(t)$, where δ is a small separation vector of initial length $||\delta_0||$. The divergence between these two points can be expressed by $||\delta(t)|| \sim ||\delta_0||e^{\ell t}$, where ℓ is the Lyapunov exponent [Str94]. A positive value of ℓ indicates that the two points on the trajectory are pushing away from each other. In other words, a positive Lyapunov exponent means that two nearby points are rapidly diverging from each other, implying a sensitive dependence on initial conditions. Thus, if we can find one positive Lyapunov exponent, the system will be chaotic [Str94]. The computation of the Lyapunov exponents requires both the solution to the system of differential equations and its linearization. Numerical methods are often used to compute the Lyapunov exponents [Mei07].

2.7 Numerical Analysis

Nonlinear problems are difficult to solve. In most cases, nonlinear systems are impossible to solve analytically. When a system cannot be solved analytically, we must implement numerical methods to formulate an approximation to the

solution. The nonlinear system used to model the dynamics of the spring-block model is a stiff system [EL08]. Stiff systems have rapid changing solutions as parameters are varied [Hol07]. The most popular numerical methods for stiff problems are the backward difference formulas (BDF). Together with a modified Newton's method, the BDF methods are implemented to solve nonlinear systems, $\mathbf{y}' = \mathbf{f}(t, \mathbf{y})$, numerically [AP98]. Using a second order BDF, $\mathbf{y}'$ can be approximated by

$$\mathbf{y}' = \frac{3\mathbf{y}_n - 4\mathbf{y}_{n-1} + \mathbf{y}_{n-2}}{2h} \tag{2.5}$$

[EL08]. We can obtain $\mathbf{y}_2$ from the initial condition $\mathbf{y}_1$ by using Euler's method

$$\mathbf{y}_2 = \mathbf{y}_1 + h * \mathbf{f}(t_1, \mathbf{y}_1). \tag{2.6}$$

Now that we have $\mathbf{y}_1$ and $\mathbf{y}_2$, we are ready to implement the BDF scheme

$$3\mathbf{y}_n - 4\mathbf{y}_{n-1} + \mathbf{y}_{n-2} = 2h\mathbf{f}(t_n, \mathbf{y}_n) \tag{2.7}$$

$$\implies 3\mathbf{y}_n - 4\mathbf{y}_{n-1} + \mathbf{y}_{n-2} - 2h\mathbf{f}(t_n, \mathbf{y}_n) = 0. \tag{2.8}$$

We rewrite the scheme as above, setting it equal to zero. This allows us to apply Newton's method at each time step to solve the root problem. Let

$$g(\mathbf{y}_n) = 3\mathbf{y}_n - 4\mathbf{y}_{n-1} + \mathbf{y}_{n-2} - 2h\mathbf{f}(t_n, \mathbf{y}_n) \tag{2.9}$$

$$\implies g'(\mathbf{y}_n) = 3I - 2hD\mathbf{f}(t_n, \mathbf{y}_n) \tag{2.10}$$

where $D\mathbf{f}$ is the Jacobian of $\mathbf{f}$. Applying Newton's method to the function $g(\mathbf{y}_n)$ for each fixed time step n, we find the $(\nu + 1)th$ Newton iteration is given by

$$\mathbf{y}_n^{\nu+1} = \mathbf{y}_n^{\nu} - (3I - 2hD\mathbf{f}(t_n, \mathbf{y}_n^{\nu}))^{-1}(3\mathbf{y}_n^{\nu} - 4\mathbf{y}_{n-1} + \mathbf{y}_{n-2} - 2h\mathbf{f}(t_n, \mathbf{y}_n^{\nu})) \tag{2.11}$$

[EL08]. In the work to follow, we will apply (2.11) to our system.

2.8 Mollifiers

The BDF (2.11) requires the computation of the Jacobian. In Chapter 4, we introduce the modified system which has a piecewise defined, discontinuous friction function. This discontinuous function poses a problem when attempting to compute the Jacobian. In order to compute the Jacobian, we must take derivatives, which means we need to be working with smooth, continuous functions. To make each equation in the system differentiable, we must approximate the piecewise function with a smooth, continuous function. We make this approximation using a mollifier. A mollifier is a smoothing equation satisfying three properties. For details on these properties see Hormander[Hor90]. The mollifier we choose to use is

$$\varphi(x) = \begin{cases} exp\left(\frac{-1}{1-x^2}\right) & \text{if } |x| < 1 \\ 0 & \text{if } |x| \geq 1. \end{cases}$$

Let $f(x)$ be the function we are trying to approximate. Using a convolution of f and φ, our smoothing function is defined as

$$\Phi_\varepsilon(f)(x) = \int_{\mathbb{R}} \varphi_\varepsilon(x-y) f(y) dy \tag{2.12}$$

where

$$\varphi_\varepsilon(x) = \varepsilon^{-1} \varphi\left(\frac{x}{\varepsilon}\right) \tag{2.13}$$

[Fri44]. In Chapter 4, we will apply the method above to our modified system.

Chapter 3

Spring-Block Model with Dieterich-Ruina Friction

To simulate the motion of the spring-block model in Figure 1.1, we consider the single degree of freedom oscillator presented in the Erickson et al. paper [EL08]. Using Dieterich-Ruina rate and state dependent friction, the equations of motion are as follows

$$\dot{\theta} = -\frac{v}{D_c}\left(\theta + Blog\left(\frac{v}{v_0}\right)\right) \tag{3.1}$$

$$\dot{u} = v - v_0 \tag{3.2}$$

$$\dot{v} = -\frac{1}{M}\left(ku + \theta + Alog\left(\frac{v}{v_0}\right)\right), \tag{3.3}$$

where θ, u, and v are the state variable, slip, and velocity, respectively. In this system, the slip of the slider-block is considered relative to the driver plate. The spring-block model represented by this system is analogous to one-dimensional earthquake motion. M is the mass of the spring block and k is the spring constant, which represents the elastic properties of the rock adjacent to the fault. D_c is the critical sliding distance, which according to Dieterich, is the slip necessary to renew asperities [Mar98]. A and B are empirical constants relating to friction stress [EL08].

3.1 Nondimensionalization of the System

By defining new dimensionless variables $\hat{\theta}$, $\hat{v}$, $\hat{u}$, $\hat{t}$ and by setting $\theta = A\hat{\theta}$, $v = v_0\hat{v}$, $u = D_c\hat{u}$, and $t = \left(\frac{D_c}{v_0}\right)\hat{t}$, we can non-dimensionalize the system of equations (3.1), (3.2), and (3.3) [EL08]. We will start with (3.1). We first find $\dot{\theta}$ in terms of the dimensionless time, $\hat{t}$, and then proceed by substituting the dimensionless parameters into (3.1) and solving for $\hat{\theta}$, as follows,

$$\dot{\theta} = \frac{d\theta}{dt} = \frac{d\theta}{d\hat{t}}\frac{d\hat{t}}{dt} = \left(\frac{Av_0}{D_c}\right)\frac{d\hat{\theta}}{d\hat{t}} \tag{3.4}$$

$$\implies \left(\frac{Av_0}{D_c}\right)\frac{d\hat{\theta}}{d\hat{t}} = \frac{-v_0\hat{v}}{D_c}\left(A\hat{\theta} + B\log\left(\frac{v_o\hat{v}}{v_0}\right)\right) \tag{3.5}$$

$$\implies \frac{d\hat{\theta}}{d\hat{t}} = -\hat{v}\left(\hat{\theta} + \frac{A}{B}\log(\hat{v})\right) \tag{3.6}$$

$$= -\hat{v}\left(\hat{\theta} + \left(\frac{B}{A} + \frac{A}{A} - \frac{A}{A}\right)\log(\hat{v})\right) \tag{3.7}$$

$$= -\hat{v}\left(\hat{\theta} + \left(1 + \frac{B-A}{A}\right)\log(\hat{v})\right) \tag{3.8}$$

$$\implies \dot{\hat{\theta}} = -\hat{v}\left(\hat{\theta} + (1+\epsilon)\log(\hat{v})\right) \tag{3.9}$$

$$\text{where } \epsilon = \frac{B-A}{A}. \tag{3.10}$$

Similarly, for (3.2) and (3.3),

$$\dot{u} = \frac{du}{dt} = \frac{du}{d\hat{t}}\frac{d\hat{t}}{dt} = v_0\frac{d\hat{u}}{d\hat{t}} \tag{3.11}$$

$$\begin{aligned}
\implies \quad v_0\frac{d\hat{u}}{d\hat{t}} &= v_0\hat{v} - v_0 \\
\implies \quad \frac{d\hat{u}}{d\hat{t}} &= \hat{v} - 1 \\
\implies \quad \dot{\hat{u}} &= \hat{v} - 1
\end{aligned}$$

$$\dot{v} = \frac{dv}{dt} = \frac{dv}{d\hat{t}}\frac{d\hat{t}}{dt} = \left(\frac{v_0^2}{D_c}\right)\frac{d\hat{v}}{d\hat{t}} \tag{3.12}$$

$$\implies \left(\frac{v_0^2}{D_c}\right)\frac{d\hat{v}}{d\hat{t}} = \left(-\frac{1}{M}\right)\left[kD_c\hat{u} + A\hat{\theta} + A\log\left(\frac{v_0\hat{v}}{v_0}\right)\right] \tag{3.13}$$

$$\implies \frac{d\hat{v}}{d\hat{t}} = \left(-\frac{D_c}{v_0^2 M}\right)\left[kD_c\hat{u} + A\hat{\theta} + A\log(\hat{v})\right] \tag{3.14}$$

$$= \left(-\frac{kD_c^2}{v_0^2 M}\right)\left[\hat{u} + \left(\frac{A}{kD_c}\right)(\hat{\theta} + \log(\hat{v}))\right] \tag{3.15}$$

$$= -\left(\frac{k}{M}\right)\left(\frac{D_c}{v_0}\right)^2\left[\hat{u} + \left(\frac{A}{kD_c}\right)(\hat{\theta} + \log(\hat{v}))\right] \tag{3.16}$$

$$\implies \dot{v} = -\gamma^2\left[\hat{u} + \left(\frac{1}{\xi}\right)(\hat{\theta} + \log(\hat{v}))\right] \tag{3.17}$$

$$\text{where } \gamma = \frac{D_c}{v_0}\sqrt{\frac{k}{M}} \text{ and } \xi = \frac{kD_c}{A}. \tag{3.18}$$

For convenience we will return to the use of θ, v, u, and t. The non-dimensional system now has the form,

$$\dot{\theta} = -v(\theta + (1+\epsilon)\log(v)) \tag{3.19}$$

$$\dot{u} = v - 1 \tag{3.20}$$

$$\dot{v} = -\gamma^2\left[u + \frac{1}{\xi}(\theta + \log(v))\right], \tag{3.21}$$

where ϵ is a measure of the sensitivity to velocity relaxation, ξ is the nondimensional spring constant, and γ is the nondimensional frequency [EL08]. We will refer to this system as (3.19) – (3.21).

3.2 The Stationary Solution

To find any stationary solutions, or fixed points of the nondimensional system (3.19) – (3.21) , we must find solutions that satisfy

$$\dot{\theta} = 0$$

$$\dot{u} = 0$$

$$\dot{v} = 0.$$

Examining (3.20), we find

$$\dot{u} = 0 \Longrightarrow v - 1 = 0 \Longrightarrow v = 1. \tag{3.22}$$

Setting $\dot{\theta} = 0$ and substituting $v = 1$ into (3.19) yields

$$\dot{\theta} = 0 \Longrightarrow -1(\theta + (1 + \epsilon)\log(1)) = 0 \Longrightarrow \theta = 0. \tag{3.23}$$

Setting $\dot{v} = 0$ and substituting $v = 1$ and $\theta = 0$ into (3.21) yields

$$\dot{v} = 0 \Longrightarrow -\gamma^2\left[u + \frac{1}{\xi}(0 + \log(1))\right] = 0 \Longrightarrow u = 0. \tag{3.24}$$

Hence the system has one fixed point at $(\theta, u, v) = (0, 0, 1)$. This fixed point represents steady sliding which in terms of the model means the block and the driver plate are moving at the same rate. The block is not moving relative to the driver plate and thus the slip is zero [EL08].

3.3 Eigenvalue Analysis

By examining the Jacobian matrix at the stationary solution, we can determine any changes in stability of the system. Particularly, the eigenvalues of this matrix will

help determine what parameter values lead to bifurcations of the fixed point. The Jacobian matrix for the non-dimensional system is

$$J = \begin{pmatrix} \frac{\partial \dot{\theta}}{\partial \theta} & \frac{\partial \dot{\theta}}{\partial u} & \frac{\partial \dot{\theta}}{\partial v} \\ \frac{\partial \dot{u}}{\partial \theta} & \frac{\partial \dot{u}}{\partial u} & \frac{\partial \dot{u}}{\partial v} \\ \frac{\partial \dot{v}}{\partial \theta} & \frac{\partial \dot{v}}{\partial u} & \frac{\partial \dot{v}}{\partial v} \end{pmatrix} = \begin{pmatrix} -v & 0 & -\theta - (1+\epsilon)(1+\log(v)) \\ 0 & 0 & 1 \\ -\frac{\gamma^2}{\xi} & -\gamma^2 & -\left(\frac{\gamma^2}{\xi}\right)\left(\frac{1}{v}\right) \end{pmatrix}. \tag{3.25}$$

Let A be the Jacobian matrix evaluated at the fixed point $(0, 0, 1)$. Then,

$$A = \begin{pmatrix} -1 & 0 & -(1+\epsilon) \\ 0 & 0 & 1 \\ -\frac{\gamma^2}{\xi} & -\gamma^2 & -\frac{\gamma^2}{\xi} \end{pmatrix}. \tag{3.26}$$

To compute the eigenvalues of the system (3.19) – (3.21), we begin by finding the characteristic equation of A, as described in Section 2.2. The characteristic equation of A is found to be

$$\lambda^3 + \lambda^2\left(1 + \frac{\gamma^2}{\xi}\right) + \lambda\left(\gamma^2 - \frac{\gamma^2\epsilon}{\xi}\right) + \gamma^2 = 0. \tag{3.27}$$

We can simplify the above expression as follows,

$$\lambda^3 + c_2\lambda^2 + c_1\lambda + c_0 = 0 \tag{3.28}$$

where

$$c_2 = 1 + \frac{\gamma^2}{\xi} \tag{3.29}$$

$$c_1 = \gamma^2 - \frac{\gamma^2\epsilon}{\xi} \tag{3.30}$$

$$c_0 = \gamma^2. \tag{3.31}$$

Now, finding the eigenvalues of A is equivalent to finding the roots of the cubic equation (3.28). As demonstrated by Zhao and Milner [ZM08], we can use the cubic formula from algebra to determine the types of roots of a polynomial in terms of their discriminant. The following lemma can be found in many algebra textbooks.

Lemma 3.1 *Let $x^3 + c_2x^2 + c_1x + c_0$ be a third order polynomial and define its discriminant as*

$$\bar{D} = \left(\frac{3c_1 - c_2^2}{9}\right)^3 + \left(\frac{9c_1c_2 - 27c_0 - 2c_2^3}{54}\right)^2.$$

If $\bar{D} > 0$, one root of the polynomial is real and two are complex conjuagtes; if $\bar{D} = 0$, all roots are real and at least two are equal; and if $\bar{D} < 0$, all roots are real and unequal [ZM08].

By Lemma 3.1, the discriminant of (3.28) is

$$\bar{D} = \left(\frac{3\left(\gamma^2 - \frac{\gamma^2\epsilon}{\xi}\right) - \left(1 + \frac{\gamma^2}{\xi}\right)^2}{9}\right)^3 + \left(\frac{9\left(\gamma^2 - \frac{\gamma^2\epsilon}{\xi}\right)\left(1 + \frac{\gamma^2}{\xi}\right) - 27\left(\gamma^2\right) - 2\left(1 + \frac{\gamma^2}{\xi}\right)^3}{54}\right)^2. \tag{3.32}$$

The transition to chaos for the system is controlled by ϵ [EL08], so we will be interested in varying the parameter ϵ. For fixed values of γ and ξ, we can view the discriminant as a function of epsilon. This allows us to determine the value of the discriminant for various values of ϵ. We find that for small values of ϵ, $\bar{D} < 0$, implying the existence of one real eigenvalue and two complex conjugate eigenvalues. Fix $\gamma = 0.8$ and $\xi = 0.8$ and consider ϵ. Plotting the discriminant versus ϵ for these values we can see that when $\epsilon \approx 3.4$, $\bar{D} = 0$. See Figure 3.1.

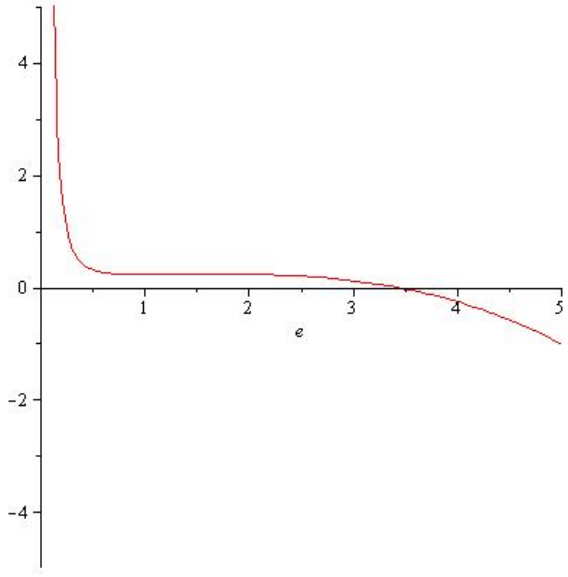

Figure 3.1: Discriminant Plot for $(\epsilon, \xi, \gamma) = (\epsilon, 0.8, 0.8)$

Hence, for $\epsilon < 3.4$ the system (3.19) – (3.21) has one real eigenvalue and a pair of complex conjugate eigenvalues. To further investigate the eigenvalues of A we can plot the eigenvalues as a function of ϵ, as seen in Figures 3.2 and 3.4. From the plot in Figure 3.2, it is clear that when A has a pair of complex conjugate eigenvalues the other eigenvalue is negative. Since the system has a pair of complex conjugates and a non-zero real eigenvalue, there is a possibility that the system undergoes a Hopf bifurcation. For a Hopf bifurcation to occur, the real part of the complex eigenvalues must cross the imaginary axis. Namely, we want the sign on the real part of the complex values to change. Using the same parameter values, we plot the real part of the eigenvalues in Figure 3.3. Analyzing the plot, it is clear that a Hopf bifurcation occurs. The real eigenvalue remains negative while the complex conjugate pair begins with a negative real part and then crosses the x-axis around $\epsilon = 0.39$, changing the real part to a positive value. For $\epsilon < 0.39$, the system has

a spiral sink near the fixed point since all of the eigenvalues have a negative real part. When eigenvalues cross the imaginary axis, the fixed point loses its stability and a periodic orbit surrounding the fixed point is born from the fixed point. We run a similar analysis for the values $\gamma = 100$ and $\xi = 1$ and again find that the system undergoes a Hopf bifurcation. See Figures 3.4 and 3.5. Note that in both of these figures, a real eigenvalue exists at a value of approximately -10^4, but due to scaling is not in the plot.

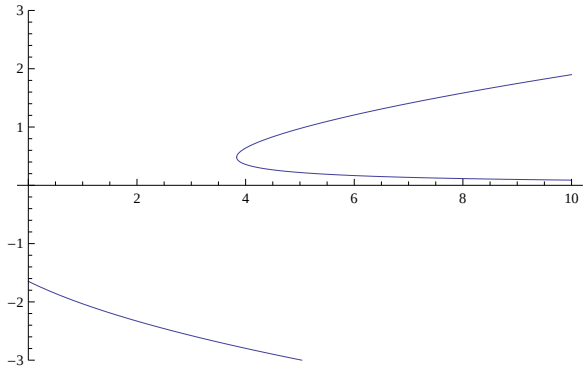

Figure 3.2: Eigenvalues for $(\epsilon, \xi, \gamma) = (\epsilon, 0.8, 0.8)$

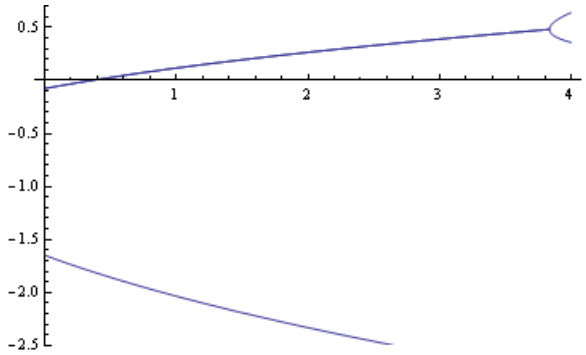

Figure 3.3: Real part of Eigenvalues for $(\epsilon, \xi, \gamma) = (\epsilon, 0.8, 0.8)$

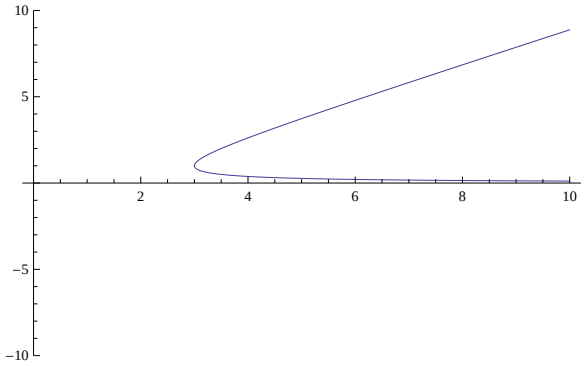

Figure 3.4: Eigenvalues for $(\epsilon, \xi, \gamma) = (\epsilon, 1, 100)$

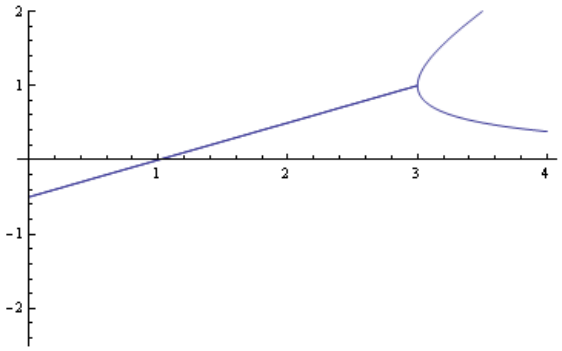

Figure 3.5: Real part of Eigenvalues for $(\epsilon, \xi, \gamma) = (\epsilon, 1, 100)$

In general, for a fixed ξ and γ, we find that the system begins with one negative eigenvalue and a pair of complex conjugate eigenvalues with negative real part. As ϵ is increased, the real part of the complex eigenvalues becomes positive and the system undegoes a Hopf bifurcation. It appears that the larger the value of γ, the more negative the real eigenvalue becomes. These figures agree with the observation that Erickson et al. made; as γ is increased, the minimum eigenvalue decays toward negative infinity [EL08]. This is important because as the eigenvalues become more negative, the system becomes stiffer. Erickson et al. cited realistic values of γ in the range of $10^4 - 10^{12}$ [EL08].

3.4 Numerical Methods

Since the system is stiff, popular numerical methods such as Euler's method and explicit Runge-Kutta, are numerically unstable, requiring very small time steps to ensure numerical stability [AP98], [EL08]. Mathematical computing software has built in numerical solvers for systems of ordinary differential equations. Using basic built in solvers in Mathematics and Maple yielded poor results for the system. In MATLAB, certain solvers, such as ode23 and ode23tb, which are based off of a trapezoidal rule and an implicit Runge-Kutta respectively, are intended for solving stiff systems. According to MathWorks, the best accuracy and fastest simulation speed is typically achieved with ode23tb for stiff systems [Inc12]. Applying the ode23tb solver to the nondimensional system produced reasonable results for small values of ϵ and γ. For larger values of ϵ and γ, MATLAB warned that the system was encountering imaginary parts in its computations. The imaginary values

found with the ode23tb solver indicate that the step size must be smaller. When the velocity value approaches 0, problems can arise if the step size is not small enough. When the step size is too large, the velocity may assume zero or negative values, consequently producing imaginary or undefined values for $\log(v)$ and an inaccurate solution to the problem. Thus, we must write our own scheme, one in which we can control the step size. Erickson et al. had success using a backward differentiation formula, and thus we choose to use a BDF as well. We implement (2.11) from the preliminaries

$$\mathbf{y}_n^{\nu+1} = \mathbf{y}_n^{\nu} - (3I - 2hD\mathbf{f}(t_n, \mathbf{y}_n^{\nu}))^{-1}(3\mathbf{y}_n^{\nu} - 4\mathbf{y}_{n-1} + \mathbf{y}_{n-2} - 2h\mathbf{f}(t_n, \mathbf{y}_n^{\nu})) \tag{3.33}$$

where

$$\mathbf{y}_n^{\nu} = \begin{bmatrix} \theta_n^{\nu} \\ u_n^{\nu} \\ v_n^{\nu} \end{bmatrix} \tag{3.34}$$

$$\mathbf{f}(t_n, \mathbf{y}_n^{\nu}) = \begin{bmatrix} -v_n^{\nu}(\theta_n^{\nu} + (1+\epsilon)\log(v_n^{\nu}) \\ v_n^{\nu} - 1 \\ -\gamma^2(u_n^{\nu} + \frac{1}{\xi}(\theta_n^{\nu} + \log(v_n^{\nu})) \end{bmatrix} \tag{3.35}$$

$$D\mathbf{f} = \begin{bmatrix} -v_n^{\nu} & 0 & -\theta_n^{\nu} - (1+\epsilon)(\log(v_n^{\nu}) + 1) \\ 0 & 0 & 1 \\ -\frac{\gamma^2}{\xi} & -\gamma^2 & \left(-\frac{\gamma^2}{\xi}\right)\left(\frac{1}{v_n^{\nu}}\right) \end{bmatrix} \tag{3.36}$$

[EL08]. See the appendix for the MATLAB code, BDF.m, for implementing this scheme.

Although the BDF is a stable scheme, we still have to deal with the nonlinearity of the logarithmic term. Our time step is restricted despite the stability of the

scheme. High values of γ will restrict our step size to an even smaller value [EL08]. Taking the time step small enough will result in the the velocity value being positive. Like with ode23tb, our scheme will become inaccurate if the time step is too large.

3.5 Numerical Simulations

Solving the system numerically, we find that varying the parameter values, (ϵ, ξ, γ), changes the dynamics of the system. When ϵ is small, numerical simulations result in either stationary solutions or orbits of period one or two. Erickson used a Poincaré map to construct a bifurcation diagram for the system as ϵ is varied [EL08]. The system begins with an attracting fixed point. As the system undergoes a Hopf bifurcation, an attracting period one orbit is produced from the fixed point. When the period one orbit is born, the fixed point exists in the system but is no longer stable. The attracting periodic orbit is verified by the attracting fixed point for the Poincaré map. In the bifurcation diagram, the fixed point representing the period one orbit bifurcates into two points, corresponding to a periodic orbit that has "split" into a longer cycle. The period two orbit is attracting, whereas the period one orbit is now unstable. Period-doubling bifurcations continue, eventually leading to a region where chaos emerges [EL08]. The random distribution of points on a Poincaré map represents chaotic behavior. Once the system is chaotic, all periodic orbits and fixed points are unstable.

While we were not able to construct a bifurcation diagram of our own, we can use numerical simulations to prove that the bifurcations occur. We can confirm the

occurrence of a Hopf bifurcation for fixed $\xi = 0.8$ and $\gamma = 0.8$ as ϵ is varied from 0.2 to 1.9 by plotting the corresponding phase space for each ϵ. Figures 3.6 and 3.7 represent a stationary solution, whereas Figures 3.10 and 3.11, show a solution after the Hopf bifurcation has occurred. Similarly, Figure 3.9 shows a spiral sink, and as ϵ is increased, a periodic orbit is born in Figure 3.13. Without the corresponding Poincaré map, we cannot determine the period of the orbit. However, in order for the orbits of period two or higher in the period-doubling cascade to exist, a period one orbit must have existed and been stable for some range of epsilon. Hence, in each case the system has undergone a Hopf bifurcation.

Figures 3.7 and 3.9 represent a stationary solution. In both cases, all the eigenvalues have a negative real part, resulting in a spiral sink near the fixed point. The spiral sink in the phase space indicates that trajectories are moving toward the fixed point $(0, 0, 1)$ as time progresses. In the corresponding time series plots of θ, u, and v versus time we can see that each value oscillates and then eventually settles to the fixed point. See Figures 3.6 and 3.8. As time passes, the velocity becomes constant at $v = 1$. Here, the velocity of the block is the same as the velocity of the driver plate; steady sliding. The slip of the block relative to the driver plate becomes zero, as does the state variable (asperity contact). Physically, the block is sliding at the same rate as the driver plate so no slip is occurs [EL08].

Periodic orbits can be observed in the phase space of Figures 3.11 and 3.13. The orbits are of at least period one. The corresponding time series plots describe the relationship between the state variable, slip, and velocity at any given time. As the velocity reaches it maximum, the slip increases. Then, as the velocity approaches zero, the slip decreases. Physically, the block is approaching its maximum

displacement ahead of the block when the velocity is at its maximum. Just after the velocity reaches its minimum, the block reaches its maximum displacement behind the block. As the velocity increases, the state variable decreases. In terms of the spring-block model, the faster the block is moving, the less asperity contact the block has with the surface. It follows that the slower the block is moving, the greater the asperity contact between the block and the surface. This is represented in the time series by when the velocity approaches zero, the state variable increases. This relationship is easily recognized in the time series and the phase space for $(\theta, u, v) = (2, 1.2, 1)$, as shown in Figures 3.14 and 3.15

Numerically, we were able to simulate an attractor. See Figure 3.16. According to Erickson et al., choosing $\epsilon = 12$ should produce a strange attractor. Erickson et al. used the Fourier power spectrum to prove the attractor was chaotic [EL08]. Here we propose the use of Lyapunov exponents, as described in Section 2.6. However, the Lyapunov exponent requires the solution to (3.19) – (3.21) as well as its linearization. Recall to solve the system we implemented the BDF scheme, which required the Jacobian to be calculated at each step. The extremely small step size necessary in the numerical simulation required us to iterate the code many times, on the order of $10^5 - 10^7$. The computational cost of computing the Lyapunov exponents is expensive in this case. While we have not been able to implement a code to calculate the Lyapunov exponents, it is something we will consider in future studies. We can see that the aperiodic nature of Figure 3.17 suggests that the attractor is strange.

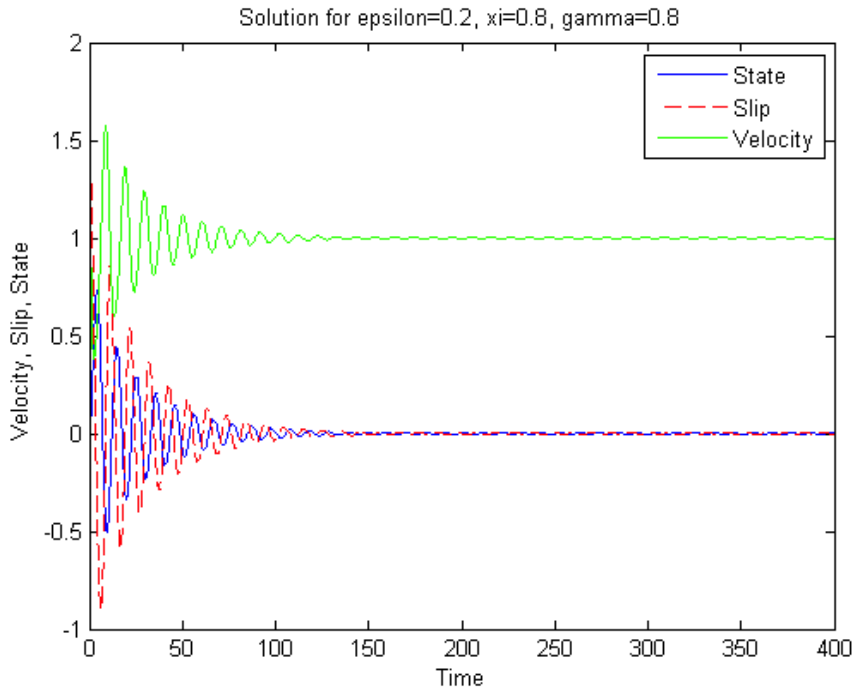

Figure 3.6: Time Series for $(\epsilon, \xi, \gamma) = (0.2, 0.8, 0.8)$

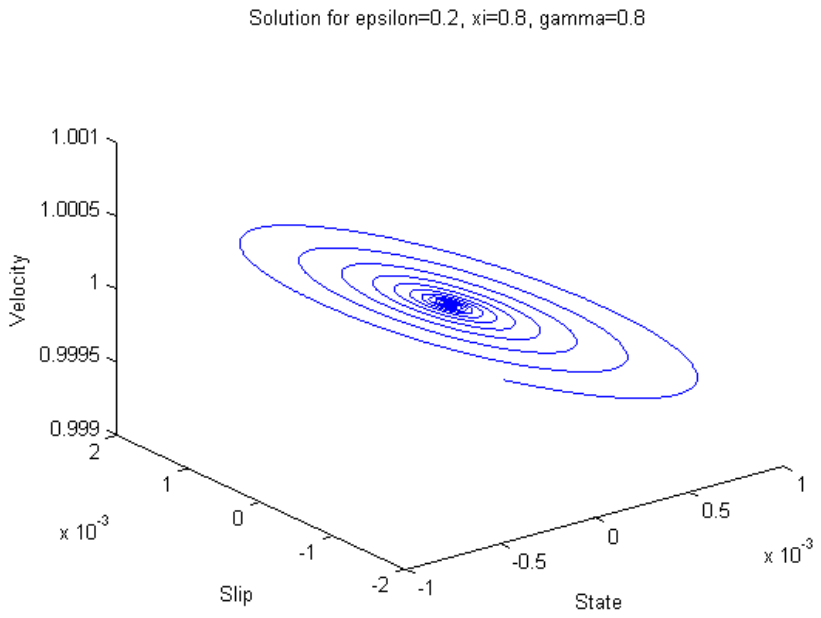

Figure 3.7: Phase Space for $(\epsilon, \xi, \gamma) = (0.2, 0.8, 0.8)$

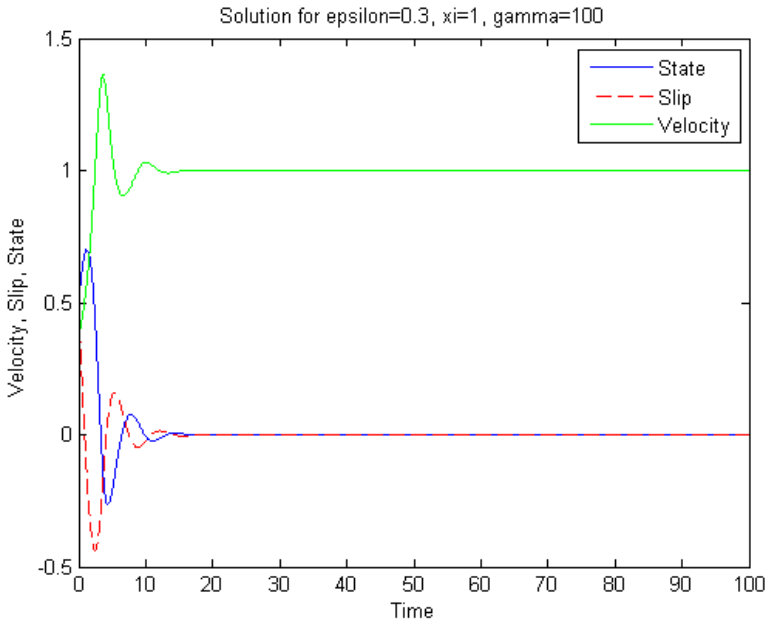

Figure 3.8: Time Series for $(\epsilon, \xi, \gamma) = (0.3, 1, 100)$

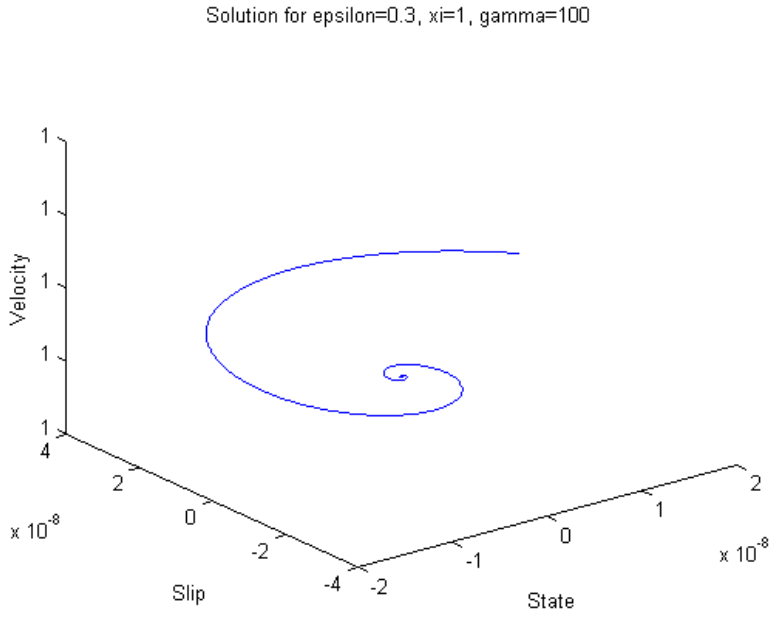

Figure 3.9: Phase Space for $(\epsilon, \xi, \gamma) = (0.3, 1, 100)$

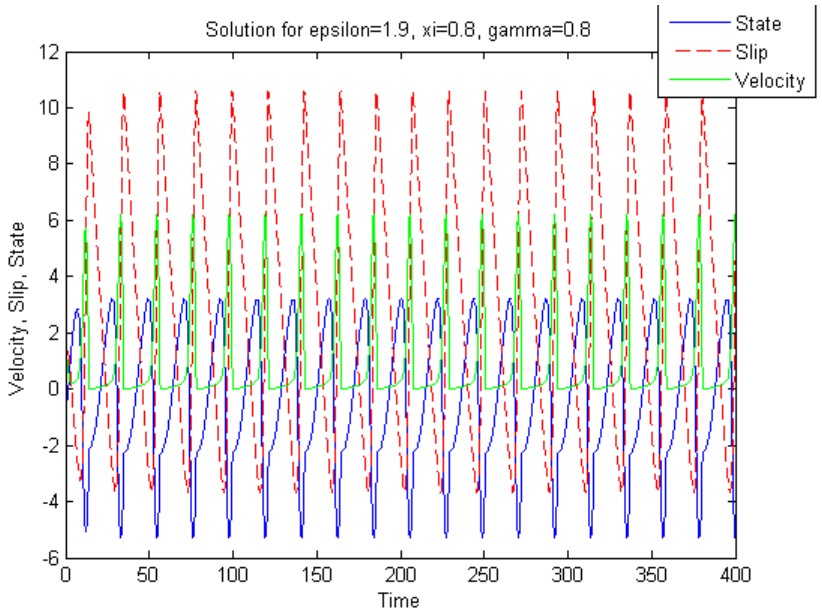

Figure 3.10: Time Series for $(\epsilon, \xi, \gamma) = (1.9, 0.8, 0.8)$

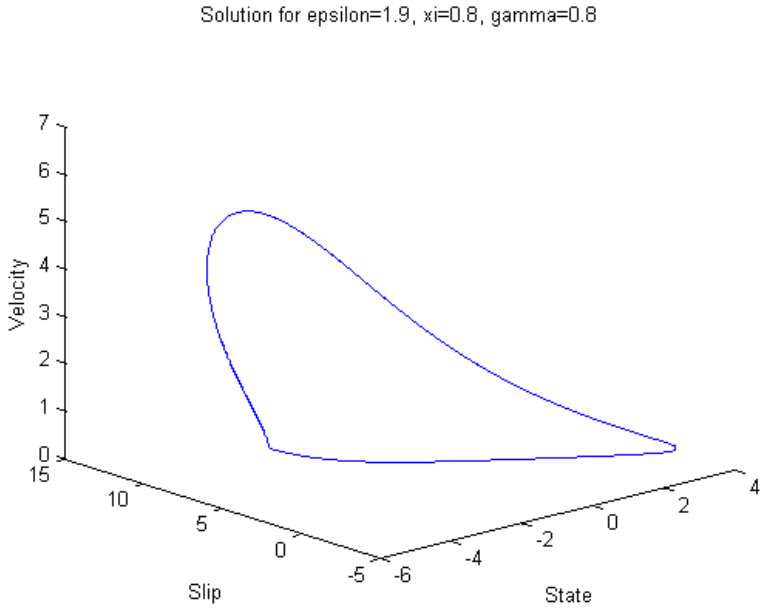

Figure 3.11: Phase Space for $(\epsilon, \xi, \gamma) = (1.9, 0.8, 0.8)$

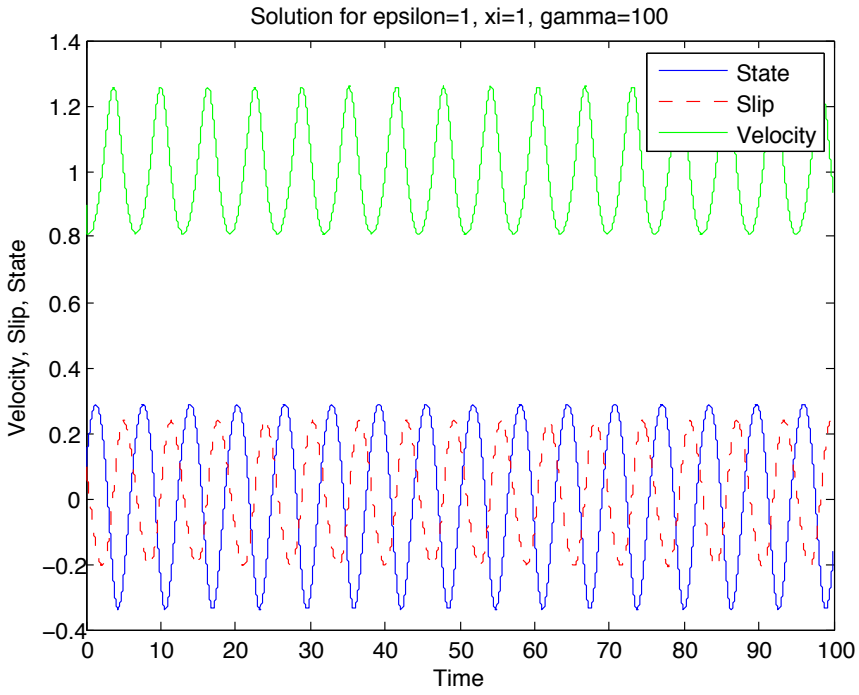

Figure 3.12: Time Series for $(\epsilon, \xi, \gamma) = (1, 1, 100)$

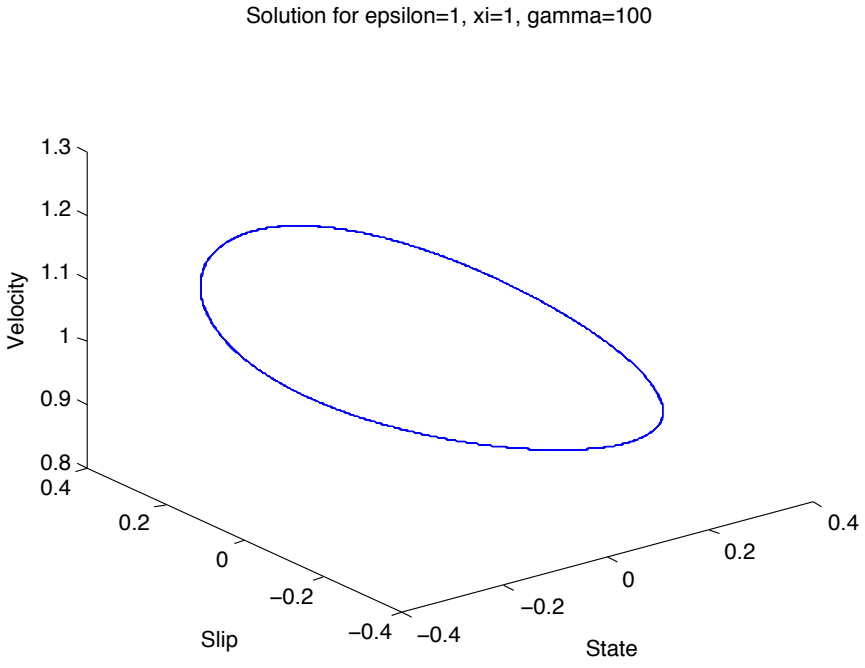

Figure 3.13: Phase Space for $(\epsilon, \xi, \gamma) = (1, 1, 100)$

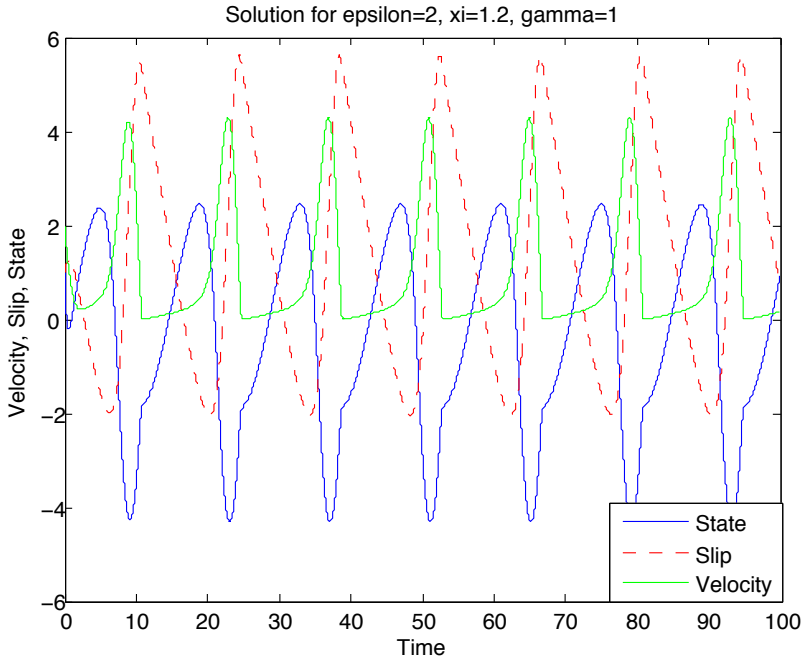

Figure 3.14: Time Series for $(\epsilon, \xi, \gamma) = (2, 1.2, 1)$

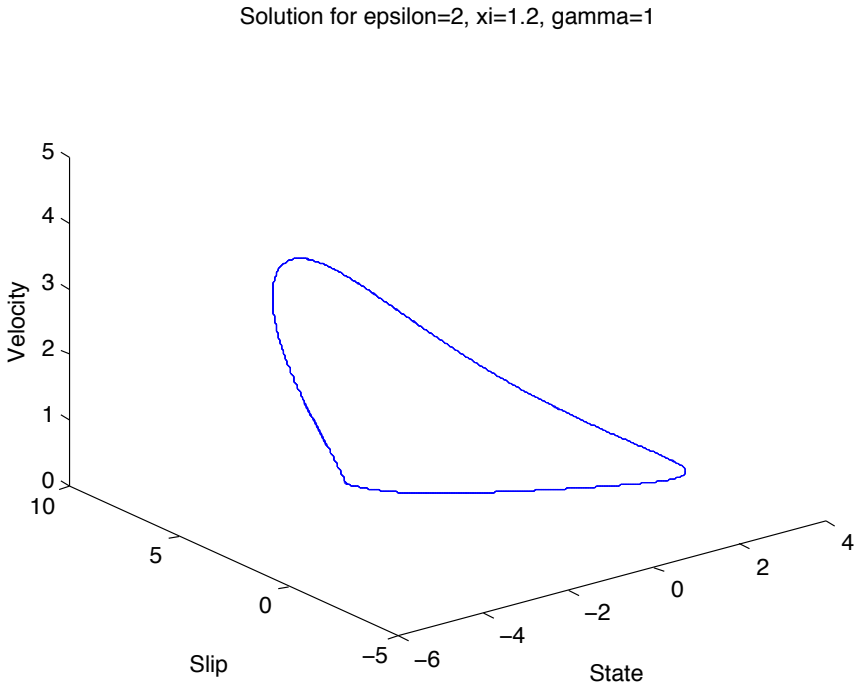

Figure 3.15: Phase Space for $(\epsilon, \xi, \gamma) = (2, 1.2, 1)$

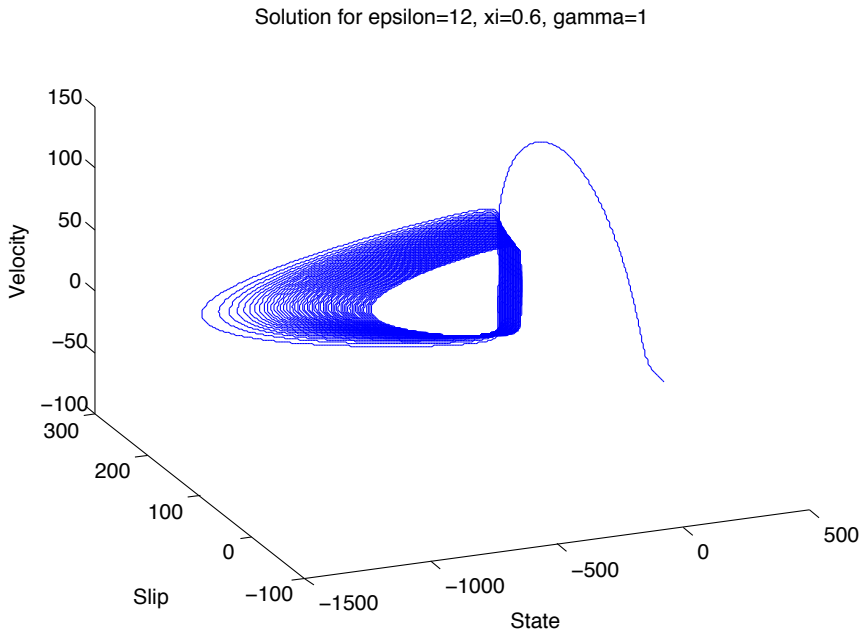

Figure 3.16: Strange Attractor for $(\epsilon, \xi, \gamma) = (12, 0.6, 1)$

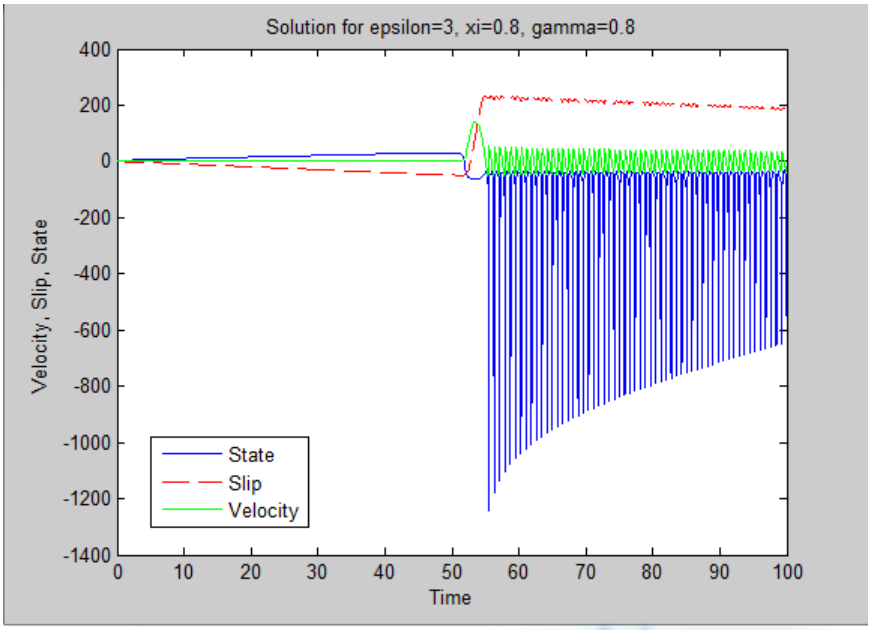

Figure 3.17: Time Series for $(\epsilon, \xi, \gamma) = (12, 0.6, 1)$

3.6 Incorporation of a Viscous Term

According to Wang [Wan07], viscosity is another important factor in earthquake rupture. Directly implementing a viscous term into a dynamical system is difficult, so Wang represented the viscosity in terms of a damping coefficient. The damping coefficient is proportional to the viscosity. We also consider a damped version of this system. Assuming the damping was due to viscosity, we introduce a damping coefficient in (3.1) – (3.3), given by,

$$\dot{\theta} = -\frac{v}{D_c}\left(\theta + Blog\left(\frac{v}{v_0}\right)\right) \tag{3.37}$$

$$\dot{u} = v - v_0 \tag{3.38}$$

$$\dot{v} = -\frac{1}{M}\left(ku + \theta + Alog\left(\frac{v}{v_0}\right) + cv\right), \tag{3.39}$$

where c is the viscous damping coefficient. We nondimensionalize the system (3.37) – (3.39) using the same substitutions as for the original system. Returning to the use of θ, u, v, and t puts the system in the form,

$$\dot{\theta} = -v(\theta + (1+\epsilon)\log(v)) \tag{3.40}$$

$$\dot{u} = v - 1 \tag{3.41}$$

$$\dot{v} = -\gamma^2\left[u + \frac{1}{\xi}(\theta + \log(v)) + \eta v\right], \tag{3.42}$$

where $\eta = \dfrac{cv_0}{kl}$ is the dimensionless viscous damping coefficient. The fixed point of this system is $(\theta, u, v) = (0, \eta, 1)$. We find that the systems (3.19) – (3.21) and (3.40) – (3.42) are the same in a qualitative sense. The systems have different fixed points, but the local behavior around each fixed point is the same. For the same reason that gravity doesn't effect the qualitative behavior of a hanging spring

in comparison to a spring in horizontal motion, the viscous term preserves the dynamic behavior of the system. In both cases, as ϵ is increased, a Hopf bifurcation occurs, followed by a series of period-doubling bifurcations into chaos.

Chapter 4

Modified System

In this chapter we consider a modified version of the system presented by Erickson et al. We propose a modification to the logarithmic term in (3.1) and (3.3). Earthquakes occur in regions of the earth that are almost universally permeated with fluids [Sch02]. Incorporating terms that account for wetness in faults, such as frictional melting, pore pressure, and viscosity, is difficult [Wan07]. We assume that the logarithmic terms remain the same as in the system in Chapter 3 up to a critical value of velocity, v_c. Once the slider-block reaches this critical velocity, each logarithmic term instantaneously dies out, assuming a value of zero. Physically, this is intended to represent some effects of a fluid within the fault. In terms of our spring-block model, the slider-block is sliding on some fluid. When v_c is reached, the fluid acts as a lubricant in the system, and hence the frictional force vanishes. Another interpretation for the vanishing of the logarithmic term may be the fault medium. For the majority of types of rocks, the friction law is independent of lithology. This is known as Byerlee's law. Several minerals, such as clays, serpentine, and talc, have a lower friction than most other rocks and minerals [Sch02]. These rocks would impact the friction in the system. Thus, encountering an area in a fault where a mineral such as talc is present may account for the sudden drop in velocity. Taking into consideration the friction drop at the critical velocity, the

modified system becomes

$$\dot{\theta} = -\frac{v}{D_c}\left(\theta + Bg\left(v/v_0\right)\right) \tag{4.1}$$

$$\dot{u} = v - v_0 \tag{4.2}$$

$$\dot{v} = -\frac{1}{M}\left(ku + \theta + Ag(v/v_0)\right), \tag{4.3}$$

where

$$g(v/v_0) = \begin{cases} \log(v/v_0) & \text{if } (v/v_0) < v_c \\ 0 & \text{if } (v/v_0) \geq v_c. \end{cases}$$

4.1 Qualitative Analysis

We nondimensionalize this system just as we did for the previous systems; setting $\theta = A\hat{\theta}$, $v = v_0\hat{v}$, $u = D_c\hat{u}$, and $t = \left(\frac{D_c}{v_0}\right)\hat{t}$. Returning to the use of θ,u, v and t puts the system into the following nondimensional form,

$$\dot{\theta} = -v(\theta + (1+\epsilon)g(v)) \tag{4.4}$$

$$\dot{u} = v - 1 \tag{4.5}$$

$$\dot{v} = -\gamma^2[u + \frac{1}{\xi}(\theta + g(v))], \tag{4.6}$$

where

$$g(v) = \begin{cases} \log(v) & \text{if } v < v_c \\ 0 & \text{if } v \geq v_c. \end{cases}$$

In our system, we assume that $v_c = 2$. By setting $(\dot{\theta}, \dot{u}, \dot{v}) = (0, 0, 0)$, we can determine any stationary solutions of the system. We find that the system has only one fixed point, $(0, 0, 1)$, which is also the fixed point for the system (3.19) – (3.21). We want to compare the qualitative features of the modified system with the original

system. For qualitative behavior of the system, we analyze the Jacobian matrix. Since the velocity at the stationary solution is less than the critical velocity, $v_c = 2$, the modified system assumes the logarithmic term for $g(v)$ near the fixed point. This puts the system into the form of (3.19) – (3.21) near the fixed point. Hence, local to the fixed point, we should see the same dynamic behavior as in Chapter 3. We expect the system to undergo a Hopf bifurcation into a series of period-doubling bifurcations leading to chaos. To confirm this conjecture, we must again run numerical simulations.

4.2 Numerical Analysis

We encounter problems trying to compute the Jacobian directly due to the discontinuity of g at v_c. The function g must be differentiable in order for the Jacobian to exist for all values in the system. Since g is a discontinuous function, we must approximate it with a smooth function. We will approximate g using a mollifier. The mollifier is given by:

$$\Phi_\varepsilon(f)(v) = \int_0^{v_c} \varphi_\varepsilon(v-y)\log(y)dy \tag{4.7}$$

where

$$\varphi_\varepsilon(v-y) = \begin{cases} \varepsilon^{-1} exp\left(\frac{-1}{1-\left(\frac{v-y}{\varepsilon}\right)^2}\right) & \text{if } \left|\frac{v-y}{\varepsilon}\right| < 1 \\ 0 & \text{if } \left|\frac{v-y}{\varepsilon}\right| \geq 1. \end{cases}$$

To solve (4.7) we must use numerical integration. Let $\tilde{f}(v) = \Phi_\delta(f)(v)$. We can rewrite our system as

$$\dot{\theta} = -v(\theta + (1+\epsilon)\tilde{f}(v)) \tag{4.8}$$

$$\dot{u} = v - 1 \tag{4.9}$$

$$\dot{v} = -\gamma^2[u + \frac{1}{\xi}(\theta + \tilde{f}(v))]. \tag{4.10}$$

Computing the Jacobian of system (4.8), (4.9), (4.10) produces

$$J = \begin{pmatrix} -v & 0 & -\theta - (1+\epsilon)(v\tilde{f}'(v) + \tilde{f}(v)) \\ 0 & 0 & 1 \\ -\frac{\gamma^2}{\xi} & -\gamma^2 & -\left(\frac{\gamma^2}{\xi}\right)\tilde{f}'(v) \end{pmatrix}. \tag{4.11}$$

The derivative of the mollifier is given by

$$\tilde{f}'(v) = \int_0^{v_c} \varphi_\varepsilon'(v-y)\log(y)dy \tag{4.12}$$

where

$$\varphi_\varepsilon'(v-y) = \begin{cases} -2\varepsilon^{-3} exp\left(\frac{-1}{1-\left(\frac{v-y}{\varepsilon}\right)^2}\right)\left(\frac{v-y}{(1-(\frac{v-y}{\varepsilon})^2)^2}\right) & \text{if } \left|\frac{v-y}{\varepsilon}\right| < 1 \\ 0 & \text{if } \left|\frac{v-y}{\varepsilon}\right| \geq 1 \end{cases}.$$

Due to the numerical integration in both the $\tilde{f}$ and $\tilde{f}'$ terms, analyzing the Jacobian becomes very difficult. Notice that both the mollifier and its derivative must be numerically integrated, since neither can be integrated analytically. We choose a quadrature method to approximate (4.7) and (4.12). See the appendix for more details on the quadrature.

Unlike in Chapter 3 where we could analytically compute eigenvalues for various parameters, here we must rely on numerical approximations. Instead of approximating the eigenvalues, we move right to numerical simulations of the

system. The modified system inherts the stiffness from the original system. Due to the stiffness, we implement the BDF scheme using the system (4.8) − (4.10) and the Jacobian (4.11). Although this code is very similar to the one implemented in the Chapter 3 simulations, it is much more computationally expensive. We must incorporate the approximation of $g(v)$ and its derivative at each iteration. To run this code efficiently, it was necessary to decrease the step size from previous simulations. The computational time for each trial significantly increased from Chapter 3 simulations. See the appendix for the code BDFm.m.

Running the simulations, we are able to produce a spiral sink, as seen in Figure 4.1. This confirms that we have a pair of complex conjugate eigenvalues with a negative part and a negative real eigenvalue. Knowing this, there is a chance a Hopf bifurcation occurs as ϵ is increased. There was some difficulty in producing plots as ϵ increased. Increasing ϵ required a reduced step size, and consequently a higher number of iterations in the coding. We were able to produce plots that looked nearly periodic. See Figure 4.2. The trajectory in the plots is not long enough to determine with certainty that the phase space is indeed periodic. Producing a strange attractor will be something that requires more time as well. With an improved code, we are hoping to be able to produce the periodic and chaotic plots to confirm our conjecture about the behavior of the modified system.

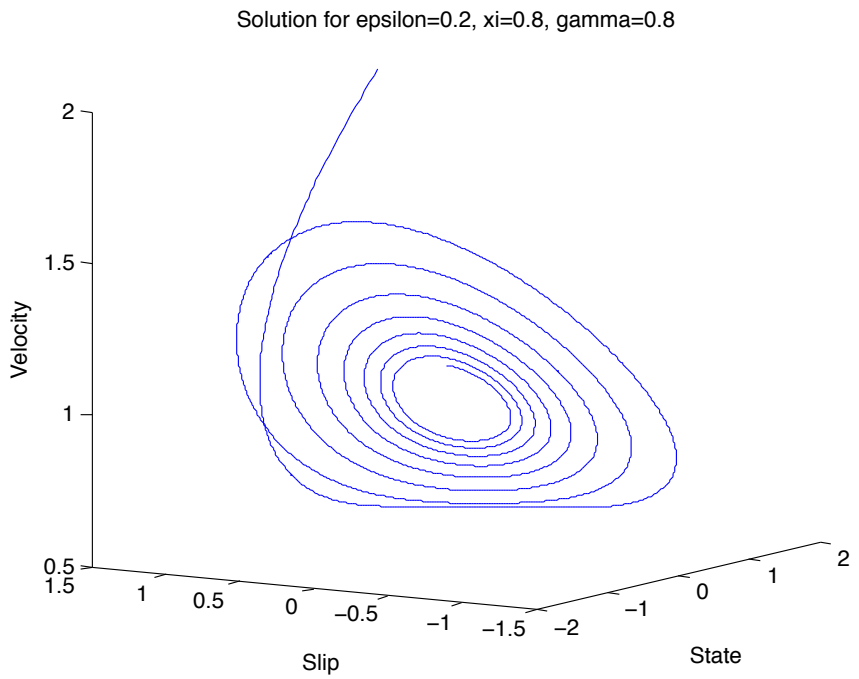

Figure 4.1: Modified System Phase Space for $(\epsilon, \xi, \gamma) = (0.2, 0.8, 0.8)$

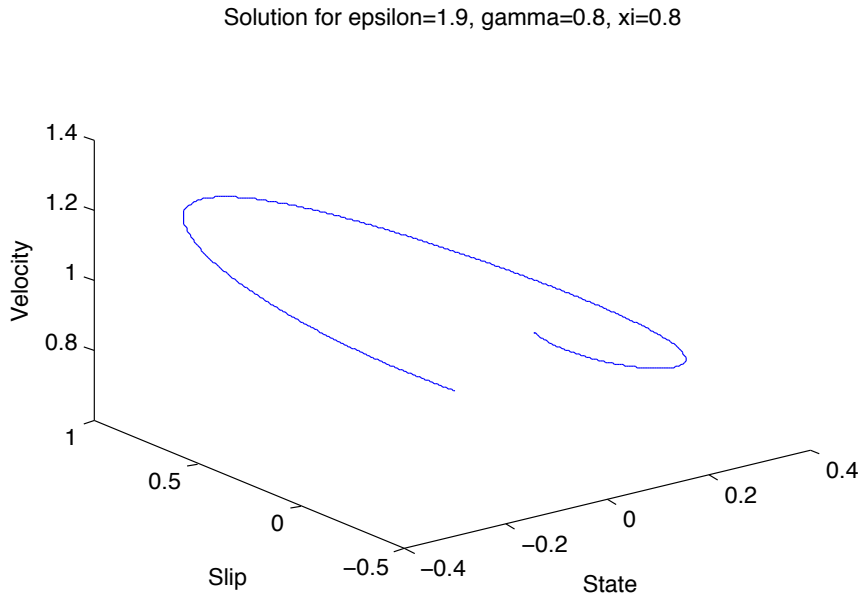

Figure 4.2: Modified System Phase Space for $(\epsilon, \xi, \gamma) = (1.9, 0.8, 0.8)$

Chapter 5

Conclusion

In this paper, we analyzed the behavior of two different spring block models. In Chapter 3, we used both qualitative analyses and numerical analyses to determine the behavior of the system. We found that the system undergoes a Hopf bifurcation and then through a series of period doubling bifurcations, which leads to chaos in the system [EL08]. In terms of the model, the chaotic region explains why predicting long term behavior for the spring-block system, or for an earthquake, is not possible. We applied similar techniques to the modified system in Chapter 4, but encountered some difficulty with numerics. We hope to be able to replicate the techniques applied to the system in Chapter 3 to the system in Chapter 4 with future research.

5.1 Future Work

In order to determine if the modified system undergoes a Hopf bifurcation and a period-doubling cascade into chaos, more research must be done. We need to improve our numerical simulations. To improve our numerical simulations, we may want to consider optimizing our code. With a more efficient algorithm, we will be able to simulate phenomena for a wider variety of parameters. We also want to

explore creating a computer program for Poincaré maps and Lyapunov exponents. As we have seen in Erickson [EL08], the computations for Poincaré maps can be executed for the system in Chapter 3. Once we have a Poincaré map, we will be able to create a bifurcation diagram and see exactly where the bifurcations occur as ϵ is varied. With these tools, we would be able to determine if our modified system becomes chaotic.

Additionally, there is interest in studying systems similar to the one presented by Erickson [EL08]. There are many different physical properties to incorporate into such a model. In one case, we incorporated a viscous term, and in another modified the friction term. In the future we may want to investigate how properties such as frictional melting or pore pressure effect the system, or consider a spring-block model representing a system of two or three dimensions.

Chapter 6

Appendix

MATLAB code for solving the system

```
%Program: BDF.m
%Title: Backward Differentiation Formula
%Description: BDF solves the diff eqn y'=f(t,y) as described in Chapter 3
%Inputs:
    %force: function
    %gradforce: Jacobian
    %epsilon: parameter
    %gamma: parameter
    %xi: parameter
    %theta(1),u(1),v(1): initial conditions
 %Outputs:
    %time series plot
    %phase space
%=========================================================================
clear;clc
global epsilon gamma xi %parameters
```

```
epsilon=2;

gamma=1;

xi=1.2;


h=0.001; %step size

TOL=1E-12;


theta(1)=1; %initial conditions

u(1)=1;

v(1)=2;


M = 100000;

y = zeros(M, 3);

% y(1,:) stands for initial data y(0)

y(1,:) = [theta(1),u(1),v(1)];

f = force(y(1,:));

Df = gradforce(y(1,:));

;

% y(2,:) apprxomiate y(h)

y(2,:) = y(1,:) + h*f;


for i = 3:M

    i

    y2n = y(i-1,:);
```

```
    y1 = y(i-1,:);
    y0 = y(i-2,:);
    for n = 1:100
        f = force(y2n);
        Df = gradforce(y2n);
        A = 3*eye(3)-2*h*Df;
        b = 3*y2n-4*y1+y0-2*h*f;
        ynew = y2n-(inv(A)*b')';
        if norm(ynew-y2n) < TOL
            break
        else
            y2n = ynew;
        end
    end
    y(i,:) = ynew;
    n
end

T=h*M;
t = 0:h:(T-h);

plot(t,y(:,1),'b',t,y(:,2), 'r--',t,y(:,3), 'g') %plot time series
xlabel('Time')
ylabel('Velocity, Slip, State ')
```

```
title('Solution for epsilon=2, xi=1.2, gamma=1')
legend('State','Slip','Velocity')

plot3(y(M/2:M,1),y(M/2:M,2),y(M/2:M,3)) %plot phase space
xlabel('State')
ylabel('Slip')
zlabel('Velocity')
title('Solution for epsilon=2, xi=1.2, gamma=1')

%=========================================================================
%Program: force.m
%=========================================================================
function f = force(y)
% y =[theta, u, v]
global epsilon gamma xi

f(1) = -y(3)*(y(1)+(1+epsilon)*log(y(3)));
f(2) = y(3)-1;
f(3) = -gamma*gamma*(y(2)+(1/xi)*(y(1)+log(y(3))));
```

```
%=========================================================================
%Program: gradforce.m
%=========================================================================
function Df = gradforce(y)
global epsilon gamma xi
Df = zeros(3, 3);

%theta=y(1)
%u=y(2)
%v=y(3)

Df(1,1) = -y(3);
Df(1,2) = 0;
Df(1,3) = -y(1) - (1+epsilon)*(log(y(3))+1);
Df(2,1) = 0;
Df(2,2) = 0;
Df(2,3) = 1;
Df(3,1) = -gamma*gamma/xi;
Df(3,2) = -gamma*gamma;
Df(3,3) = (-gamma*gamma/xi)*(1/y(3));

%=========================================================================
%=========================================================================
```

MATLAB code for solving the modified system

```
%Program: BDFm.m
%Title: Modified Backward Differentiation Formula
%Description: BDF solves the diff eqn y'=f(t,y) as described in Chapter 4
%Inputs:
    %forcem: function
    %gradforcem: Jacobian
    %mollifier: approximation to the piecewise function
    %mollifierprime: derivative of the mollifier
    %smooth: function used in mollifier
    %smoothprime: derivative of smooth
    %epsilon: parameter
    %gamma: parameter
    %xi: parameter
    %theta(1),u(1),v(1): initial conditions
 %Outputs:
    %time series plot
    %phase space
%BDFm solves the diff eqn y'=f(t,y)


clear;clc
global epsilon gamma xi %parameters


epsilon=1.9;
```

```
gamma=.8;
xi=.8;



h=0.000001;
TOL=1E-12;

theta(1)=.1; %initial conditions
u(1)=.1;
v(1)=.9;

M = 10000000;
y = zeros(M, 3);
% y(1,:) stands for initial data y(0)
y(1,:) = [theta(1),u(1),v(1)];
fm = forcem(y(1,:));
Dfm = gradforcem(y(1,:));
m=mollifier(y(3));
mp = mollifierprime(y(3));

;
% y(2,:) apprxomiate y(h)
y(2,:) = y(1,:) + h*fm;
```

```
for i = 3:M
    i
    y2n = y(i-1,:);
    y1 = y(i-1,:);
    y0 = y(i-2,:);
    for n = 1:100
        fm = forcem(y2n);
        Dfm = gradforcem(y2n);
        A = 3*eye(3)-2*h*Dfm;
        b = 3*y2n-4*y1+y0-2*h*fm;
        ynew = y2n-(inv(A)*b')';
        if norm(ynew-y2n) < TOL
            break
        else
            y2n = ynew;
        end
    end
    y(i,:) = ynew;
    n;
end


T=h*M;
t = 0:h:(T-h);
```

```
plot(t,y(:,1),'b',t,y(:,2), 'r--',t,y(:,3), 'g')
xlabel('Time')
ylabel('Velocity, Slip, State ')
title('Solution for epsilon=0.2, xi=0.8, gamma=0.8')
legend('State','Slip','Velocity')

plot3(y(M/2:M,1),y(M/2:M,2),y(M/2:M,3)) %plot later trajectory
xlabel('State')
ylabel('Slip')
zlabel('Velocity')
title('Solution for epsilon=0.2, xi=0.8, gamma=0.8')

%=========================================================================
%Program: forcem.m
%=========================================================================
function fm = forcem(y)
% y =[theta, u, v]
global epsilon gamma xi

fm(1) = -y(3)*(y(1)+(1+epsilon)*mollifier(y(3)));
fm(2) = y(3)-1;
fm(3) = -gamma*gamma*(y(2)+(1/xi)*(y(1)+mollifier(y(3))));
```

```
%=========================================================================
%Program: gradforcem.m
%=========================================================================
function Dfm = gradforcem(y)
global epsilon gamma xi
Df = zeros(3, 3);

%theta=y(1)
%u=y(2)
%v=y(3)

Dfm(1,1) = -y(3);
Dfm(1,2) = 0;
Dfm(1,3) = -y(1) - (1+epsilon)*(y(3)*mollifierprime(y(3))+mollifier(y(3)));
Dfm(2,1) = 0;
Dfm(2,2) = 0;
Dfm(2,3) = 1;
Dfm(3,1) = -gamma*gamma/xi;
Dfm(3,2) = -gamma*gamma;
Dfm(3,3) = (-gamma*gamma/xi)*(mollifierprime(y(3)));
```

```
%=========================================================================
%Program: mollifier.m
%=========================================================================
function m = mollifier(x)
epsi=0.3;
tol = [1e-3 1e-5];
if x < -epsi;
    m = 0
elseif x < epsi;
    m = quadl('smooth',0,x+epsi,tol,[],x);
elseif x < 2-epsi;
    m = quadl('smooth',x-epsi,x+epsi,tol,[],x);
elseif x < 2+epsi;
    m = quadl('smooth',x-epsi,2,tol,[],x);
else
    m = 0;

end

%=========================================================================
%Program: mollifierprime.m
%=========================================================================
function mp = mollifierprime(x)
```

```
epsi=0.3;
tol = [1e-3 1e-5];
if x < -epsi;
    mp = 0;
elseif x < epsi;
    mp = quadl('smoothprime',0,x+epsi,tol,[],x);
elseif x < 2-epsi;
    mp = quadl('smoothprime',x-epsi,x+epsi,tol,[],x);
elseif x < 2+epsi;
    mp = quadl('smoothprime',x-epsi,2,tol,[],x);
else
    mp = 0;

end
```

```
%=========================================================================
%Program: smooth.m
%=========================================================================
function phi = smooth(y,x)
epsi=0.3;

phi = epsi^(-1)*exp(-1./(1-((x-y)./epsi).^2)).*log(y);
```

```
%=========================================================================
%Program: smoothprime.m
%=========================================================================
function phiprime = smoothprime(y,x)
epsi=0.3;

phiprime = epsi^(-2)*-exp(-1./(1-((x-y)./epsi).^2)).*(-2*((x-y)./epsi))...
./(1-((x-y)./epsi).^2).^2.*log(y);

%=========================================================================
```

Bibliography

[AP98] Uri M. Ascher and Linda R. Petzold, *Computer methods for ordinary differential equations and differential–algebraic equations*, Society for Industrial and Applied Mathematics (SIAM), Philadelphia, PA, 1998. MR 1638643 (99k:65052)

[BK67] R. Burridge and L. Knopoff, *Model and theoretical seismicity*, Bulletin of the Seismological Society of America **57** (1967), no. 3, 341–371.

[EL08] Birnir B. Erickson, B. and D. Lavallée, *A model for aperiodicity in earthquakes*, Nonlinear Processes in Geophysics **15** (2008), 1–12.

[Fri44] Kurt Otto Friedrichs, *The identity of weak and strong extensions of differential operators*, Transactions of the American Mathematical Society **55** (1944), no. 1, 132–151.

[GH90] John Guckenheimer and Philip Holmes, *Nonlinear oscillations, dynamical systems, and bifurcations of vector fields*, Applied Mathematical Sciences, vol. 42, Springer-Verlag, New York, 1990, Revised and corrected reprint of the 1983 original. MR 1139515 (93e:58046)

[Hol07] Mark H. Holmes, *Introduction to numerical methods in differential equations*, Texts in Applied Mathematics, vol. 52, Springer, New York, 2007. MR 2262415 (2007e:65001)

[Hor90] Lars Hormander, *The analysis of linear partial differential operators 1*, Grundlehren der Mathematischen Wissenschaft **256 2nd ed** (1990).

[Inc12] MathWorks Inc., *Mathworks*, 1984–2012.

[LS74] C. C. Lin and L. A. Segel, *Mathematics applied to deterministic problems in the natural sciences*, Macmillan Publishing Co., Inc., New York, 1974, With material on elasticity by G. H. Handelman. MR 0368520 (51 #4761)

[Mar98] C. Marone, *Laboratory–derived friction laws and their application to seismic faulting*, Annu. Rev. Earth Planet **26** (1998), no. 1, 643–696.

[Mei07] James D. Meiss, *Differential dynamical systems*, Mathematical Modeling and Computation, vol. 14, Society for Industrial and Applied Mathematics (SIAM), Philadelphia, PA, 2007. MR 2384060 (2009b:37002)

[Sch02] Christopher H. Scholz, *The mechanics of earthquakes and faulting*, vol. Second, Cambridge University Press, Cambridge, 2002.

[Str94] Steven H. Strogatz, *Nonlinear dynamics and chaos*, Westview press, 1994.

[Tur97] Donald L. Turcotte, *Fractals and chaos in geology and geophysics*, second ed., Cambridge University Press, Cambridge, 1997. MR 1458893 (99a:86001)

[Wan07] Jeen-Hwa Wang, *A dynamic study of frictional and viscous effects on earthquake rupture: A case study of the 1999 chi-chi, taiwan, earthquake*, Bulletin of the Seismological Society of America **97** (2007), no. 4, 1233–1244.

[Wig03] Stephen Wiggins, *Introduction to applied nonlinear dynamical systems and chaos*, second ed., Texts in Applied Mathematics, vol. 2, Springer-Verlag, New York, 2003. MR 2004534 (2004h:37002)

[ZM08] Ruijun Zhao and Fabio Augusto Milner, *A mathematical model of Schistosoma mansoni in Biomph*, Bulletin of Mathematical Biology **70** (2008), 1886–1905.